Chapter 3
Entanglement Content of Many-Body States via Concurrence, Negativity and Schmidt Gap

Sougato Bose, Abolfazl Bayat, Henrik Johannesson and Pasquale Sodano

Abstract Quantum entanglement is nearly ubiquitous in equilibrium and non-equilibrium many-body states. Although it has been largely studied through the von Neumann entropy of a subsystem, which quantifies the entanglement between two complementary parts of a many-body system, this is not necessarily the only way. Here we review how some other measures can be fruitful in characterizing the entanglement content of many-body states. For example, we can look at the entangement between two individual spins through the concurrence or between two non-complementary, but in principle large, parts of a many-body system through the negativity. Alternatively, a quantity inspired through entanglement studies, but not itself a measure of entanglement, namely the Schmidt gap, can be effective as an order parameter for phase transitions in which only the entanglement structure of a many-body system changes. We exemplify using equilibrium states of short-range and impurity models and their quantum phase transitions.

S. Bose (✉) · A. Bayat
Department of Physics and Astronomy, University College London,
Gower Street, London WC1E 6BT, UK
e-mail: s.bose@ucl.ac.uk

A. Bayat
e-mail: abolfazl.bayat@ucl.ac.uk

A. Bayat
Institute of Fundamental and Frontier Sciences, University of Electronic Science and Technology of China, Chengdu 610051, China

H. Johannesson
Department of Physics, University of Gothenburg, 41296 Gothenburg, Sweden
e-mail: henrik.johannesson@physics.gu.se

P. Sodano
INFN Sezione di Perugia, Via A. Pascoli, 06123 Perugia, Italy
e-mail: pasquale.sodano01@gmail.com

International Institute of Physics, UFRN, Natal-RN 59078-400, Brazil

A. Ferraz et al. (eds.), *Strongly Coupled Field Theories for Condensed Matter and Quantum Information Theory*, Springer Proceedings in Physics 239,
https://doi.org/10.1007/978-3-030-35473-2_3

3.1 Quantum Entanglement and Its Quantification

An example of an entangled state of two spin-1/2 systems (two qubits) with states $|0\rangle$ and $|1\rangle$ is

$$|\psi^-\rangle = \frac{1}{\sqrt{2}}(|0\rangle|1\rangle - |1\rangle|0\rangle) \tag{3.1}$$

which can never be written down as a pure product of states of the individual systems such as in the form $|\chi\rangle|\phi\rangle$. A general separable (*not* entangled) state of two systems A and B is one given by the equation

$$\rho_{AB} = \sum_i P_i |\psi\rangle\langle\psi|_A \otimes |\phi\rangle\langle\phi|_B. \tag{3.2}$$

Any state which is *not* of the above form is called an entangled state.

Entanglement is a huge area of quantum information science, with several reviews such as [1]. It is a quantifiable, as well as a measurable entity. Simply stating, the "harder" it is to approximate a state as a probability distribution over products of pure states, the "higher" is its entanglement. For example, for the case of two qubits, the state $|\psi^-\rangle$ is the most entangled, whose amount is generally set to unity, while a product state of the form $|\chi\rangle|\phi\rangle$ or mixed states of the form $p|\chi_1\rangle\langle\chi_1|_A \otimes |\phi_1\rangle\langle\phi_1|_B + (1-p)|\chi_2\rangle\langle\chi_2|_A \otimes |\phi_2\rangle\langle\phi_2|_B$ have zero entanglement.

Quantification of entanglement has been accomplished in several ways. The crucial property for an entanglement measure to satisfy is that it cannot be increased between two systems held by distant parties Alice and Bob if they are solely using local operations and classical communications (LOCC). The first measure of entanglement to be introduced was the von Neumann entropy of entanglement [2]. It applies to the entanglement of two systems of arbitrary dimensions (such as when each system is a multi-qubit system), but only for pure states. This is computed by first computing the reduced density matrix ρ_A of system A from the state ρ_{AB} of the total system using the procedure $\rho_A = Tr_B(\rho_{AB})$, where $Tr_B(\,)$ denotes partial tracing over system B. The entanglement of the two systems A and B in the pure state ρ_{AB} is then given by the von Neumann entropy [2]

$$\mathscr{S} = -Tr\{\rho_A \log_2 \rho_A\}, \tag{3.3}$$

which in terms of the eigenvalues η_i of ρ_A, is $\mathscr{S} = -\sum_i \eta_i \log_2 \eta_i$. This measure has been studied and computed for a vast majority of (pure) ground states quantum many-body systems when they are divided into two complementary parts [3]. We will thus not concentrate on the von Neumann entropy in this article.

Here, we would rather concentrate on applying those measures of entanglement to condensed matter systems which are less common. They give entanglement between two non-complementary parts of a many body systems—such as well separated blocks of spins or pairs of individual spins. For the case of two qubits (e.g. spin-1/2

systems) in a mixed state, given by a density matrix ρ, its entanglement can be computed [4]. The procedure is to first compute the matrix

$$\tilde{\rho}_{AB} = \sigma_y \otimes \sigma_y \rho^*_{AB} \sigma_y \otimes \sigma_y \tag{3.4}$$

where the complex conjugate ρ^* of ρ is taken in the basis $|00\rangle$, $|01\rangle$, $|10\rangle$, $|11\rangle$. Then the entanglement can be quantified by a number called concurrence $\mathscr{E}$ given by [4]

$$\mathscr{E} = max\{0, \lambda_1 - \lambda_2 - \lambda_3 - \lambda_4\}, \tag{3.5}$$

where λ_is are the square roots of the eigenvalues of $\rho\tilde{\rho}$ in decreasing order.

However, at times you may have two larger dimensional systems in a mixed state and want to compute their entanglement—for example, for two non-complementary blocks of spins. Then it is best to use another measure of entanglement termed the negativity. The reduced density operators ρ_{AB} carry the information on the entanglement between the blocks A and B. As ρ_{AB} is a mixed state, the block entropy is inappropriate as a measure of the entanglement. We have to use instead the negativity [5, 6] $\mathscr{N} \equiv (\sum_i |a_i| - 1)$ where $|a_i|$ denote the modulus of the eigenvalues of the partial transpose $(\rho_{AB})^{T_A}$ of ρ_{AB} with respect to the subsystem A, i.e., $\langle w_i^A\, w_j^B | \rho_{AB}^{T_S} | w_k^A\, w_l^B \rangle = \langle w_k^A\, w_j^B | \rho_{AB} | w_i^A\, w_l^B \rangle$ [1]. $\{|w^S\rangle\}$ and $\{|w^E\rangle\}$ are the orthogonal basis states of A and B respectively, chosen by the DMRG procedure. This is a widely used genuine measure of quantum correlations (entanglement monotone [7]) and provides a bound to the fidelity of teleportation with a single copy of the state [8].

Moreover, we will be using another measure, which, although, is not a measure of entanglement, it does indicate, in the broadest coarse grained way, the entanglement present between two complementary halves of a pure state system. This is called the Schmidt gap. We cut the system in two parts, A and B, and write the Schmidt decomposition of a pure state, say the ground state $|GS\rangle$, as

$$|GS\rangle = \sum_k \sqrt{\lambda_k} |A_k\rangle \otimes |B_k\rangle, \quad \lambda_k \geq 0, \tag{3.6}$$

with mutually orthogonal Schmidt basis states $|A_k\rangle$ and $|B_k\rangle$. The density matrix of each part is diagonal in the Schmidt basis,

$$\rho_\alpha = \sum_k \lambda_k |\alpha_k\rangle\langle\alpha_k|, \quad \alpha = A, B. \tag{3.7}$$

with the eigenvalues $\lambda_1 \geq \lambda_2 \geq ...$ in descending order forming the entanglement spectrum (frequently defined as $\{-\ln \lambda_i\}_{i=1,2,...}$ in the literature). Then the Schmidt gap is defined as $\Delta_S = \lambda_1 - \lambda_2$ − where λ_1 and λ_2 are the two largest eigenvalues of the reduced ground state density matrix as defined above.

3.2 Concurrence Between Two Spins of a Many-Body System

As an illustration, we will first study a model of an open ended chain of four spin-1/2 particles coupled through a nearest neighbor isotropic Heisenberg interaction, so that the Hamiltonian is

$$\mathbf{H} = \sum_{i=1}^{3} \boldsymbol{\sigma}^i . \boldsymbol{\sigma}^{i+1} \tag{3.8}$$

The ground state of this chain

$$|GS\rangle = \left(\sqrt{\frac{2}{3}} |\psi^-\rangle|\psi^-\rangle - 0.1494(|00\rangle|11\rangle - |01\rangle|01\rangle - |10\rangle|10\rangle + |11\rangle|00\rangle \right) \tag{3.9}$$

is manifestly an entangled state (just looking at the form of the state is enough to spot that) and for a long time condensed matter physicists have known that the ground states of such systems are indeed entangled. What is more important, though, is the "amount" of entanglement between two spins of the system. This had not been computed till the advent of quantum information. In order to do this, we first obtain the reduced density matrix ρ_{ij} of the spins i and j. From the expression of $|GS\rangle$, it is clear that ρ_{12} for example, is a mixed state with a significant proportion (2/3) of the maximally entangled state $|\psi^-\rangle$. The entanglement between spins i and j is computed as the concurrence $\mathscr{E}$ from the formula given in Sect. 3.1. However, it is worth mentioning here that because of certain symmetries of the Heisenberg model, the concurrence $\mathscr{E}$ reduces to a very simple formula and one need not involve all elements of the reduced density matrix ρ_{ij} for the calculation of concurrence. Note that all the states involved in the expression for $|GS\rangle$ have the same number of zeros. This is a consequence of the commutation of $\mathbf{H}$ with $\sum_i \sigma_z^i$ and holds for all eigenstates of $\mathbf{H}$, and consequently also for their mixtures such as thermal states. It is then easy for the reader to verify (I leave it as an exercise here) that the density matrix ρ_{ij} cannot have any off diagonal terms (or coherence) between spaces with different values of $\sigma_z^i + \sigma_z^j$. In the standard basis $|00\rangle$, $|01\rangle$, $|10\rangle$, $|11\rangle$, ρ_{ij} will thus be of the form

$$\begin{pmatrix} x & 0 & 0 & 0 \\ 0 & y_1 & z & 0 \\ 0 & z^* & y_2 & 0 \\ 0 & 0 & 0 & w \end{pmatrix}$$

For such a simple form of ρ_{ij}, the concurrence is given by the simple formula $\mathscr{E} = 2\max\{0, |z| - \sqrt{xw}\}$.

The concurrence between spins 1 and 2 is found to be 0.866, which is quite high (the highest possible value, for a maximally entangled state, being 1). These are nearest neighbors. On the other hand, no entanglement exists between 2 and 3,

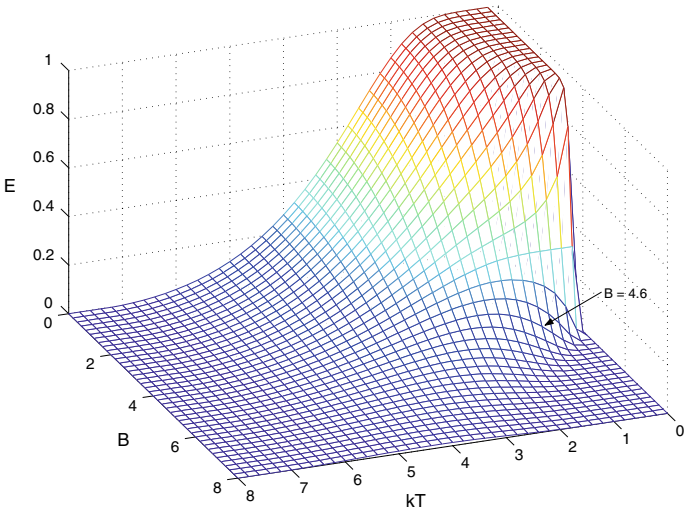

Fig. 3.1 A plot of the entanglement between two spins interacting via exchange in a magnetic field as quantified by their concurrence. It shows that entanglement ca persist at finite temperatures, and can even increase due to heating when the system is under an applied magnetic field. This latter case, while counter-intuitive, can be qualitatively understood as the ordering tendency of an external magnetic field competing with the fluctuations of the temperature to give rise to a finite entanglement

though they are nearest neighbors. The entanglement pattern of the chain is dimerized because of its open ends and there is no entanglement between any of the non-nearest neighbor spins (such as 1 and 3 or 1 and 4). Interestingly, the entanglement between two spins as quantified by concurrence can persist even in systems in a thermal state $\rho(T) = e^{-\mathbf{H}/kT}/Z$ for a system described by a Hamiltonian H at non-zero temperatures (*thermal entanglement*) and moreover, given a can also be tuned by a magnetic field. With respect to the simplest rudimentary case, namely, two spins coupled by an exchange interaction and placed in an external magnetic field,

$$\mathbf{H} = \sum_{i=1}^{N} (B\sigma_z^i + J\boldsymbol{\sigma}^i.\boldsymbol{\sigma}^{i+1}) \tag{3.10}$$

where $\boldsymbol{\sigma}^i = (\sigma_x^i, \sigma_y^i, \sigma_z^i)$ in which $\sigma_{x/y/z}^i$ are the Pauli matrices for the ith spin (we assume cyclic boundary conditions $1 + N = 1$), with $J > 0$ (antiferromagnetic interactions), the entanglement is shown as a function of the magnetic field and temperature in Fig. 3.1 which is taken from [9]. Reference [9], which was the first study of entanglement between individual spins of a spin chain in its natural (thermal/ground) state, also described the entanglement between spins of longer spin chains. Subsequently, the variation of such entanglement was also studied across *quantum phase transitions* [10]—when the ground state of certain quantum many-body systems

undergo a sudden "qualitative" change due to the variation of a parameter of the Hamiltonian. Speaking very roughly and qualitatively, the ground state near a quantum phase transition is a highly entangled state because of a competition between different ordering tendencies of different terms of a Hamiltonian. On either side of the transition different tendencies win and impose their order, while at the transition neither can win and only an entangled state can be the lowest energy state. This competition between different ordering tendencies was shown to be captured in terms of the entanglement between two spins i and j, usually nearest and next nearest neighbors, by a peak of the entanglement near the point of a quantum phase transition [11, 12].

3.3 Entanglement Negativity in a Many-Body System: Case Study with the Kondo Model

In the context of spin chains, entanglement negativity was first studied in simultaneous papers [13, 14]. For critical ground states which have no built-in scale, it was found to be *scale invariant* in the sense that it only depended on the *ratio* $\mu = x/L$ of the separation x of two noncomplementary blocks of spins in a spin chain, and the length of the blocks L (length of both the blocks are taken to be equal here). This is shown in Fig. 3.2. A combination of an exponential and a power-law dependence of the entanglement in the ratio μ was found numerically in these papers [13], while subsequently the exponential dependence has also been analytically proved [15]. Entanglement negativity can also be used for quantification of multipartite entanglement in many-body systems which also shows scaling behavior near quantum phase transition [16]. Here we will next concentrate on how the entanglement negativity can be used to extract the Kondo cloud in a spin chain emulation of the Kondo model as discussed in [17].

The simplest Kondo model [18] describes a single impurity spin interacting with the conduction electrons in a metal; the ground state is a highly nontrivial many body state in which the impurity spin is screened by conduction electrons in a large orbital of size ξ, termed as the Kondo cloud. Many physical observables vary on the characteristic length scale ξ, which is a well defined function of the Kondo coupling [18]. Determining the spatial extent of the Kondo cloud has been so far a challenging problem repeatedly addressed by various means [19, 21, 22]. This includes an investigation which introduces a quantity called "impurity entanglement entropy" which, however, is not a bonafide measure of entanglement [19, 20]. Kondo systems are expected to have a more exotic *form* of entanglement than the widely studied spin-spin and complementary block entanglements. Indeed, in Kondo systems, the impurity spin is expected to be mostly entangled with only a specific block of the whole system. This is, of course, merely an intuition which needs to be quantitatively verified with a genuine measure of entanglement: this is indeed a task that negativity can accomplish as we will elucidate in this section following [17].

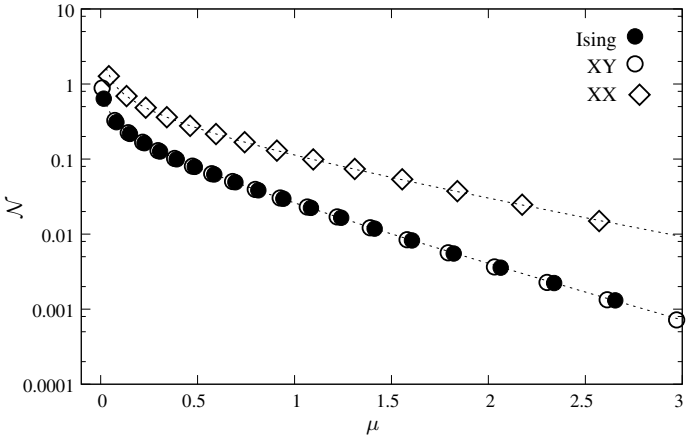

Fig. 3.2 The figure shows the dependence of the entanglement between two blocks of spins in a spin chain as quantified by the entanglement negativity. The entanglement is depicted as a function of the ratio $\mu = L/x$ of each block L and their separation x

It is known [23] that universal low energy long distance physics of this Kondo model arises also in a spin chain when a magnetic impurity is coupled to the end of a gapless Heisenberg anti-ferromagnetic $J_1 - J_2$ spin 1/2 chain, where J_1 (J_2) is the (next) nearest neighbor coupling. This is described by the Hamiltonian

$$H = J'(\sigma_1.\sigma_2 + J_2\sigma_1.\sigma_3) + \sum_{i=2}^{N-1} \sigma_i.\sigma_{i+1} + J_2 \sum_{i=2}^{N-2} \sigma_i.\sigma_{i+2}, \tag{3.11}$$

where the nearest neighbor coupling J_1 has been normalized to 1, $\sigma_i = (\sigma_i^x, \sigma_i^y, \sigma_i^z)$ is a vector of Pauli operators at site i, N is the total length of the chain. The impurity spin, located at one end of the chain, is accounted for by weaker couplings J' to the rest of the system. When J_2 exceeds a critical value, the spin chain enters a gapped dimerized regime and its relation to the Kondo model breaks down. Namely, for $0 \leq J_2 \leq J_2^c = 0.2412$, the spin system is gapless and it supports a Kondo regime [19, 20]. For $J_2 > J_2^c$, the system enters the gapped *dimer regime*, where the ground state takes a dimerised form (Fig. 3.3).

To study the entanglement of the ground state can be accomplished using DMRG as described in [17]. We determine the size of the block A when the entanglement between the impurity and block B is almost zero; by this procedure we measure an Entanglement Healing Length (EHL) L^*, i.e. the length of the block A which is maximally entangled with the impurity. We show that, in the gapless Kondo regime, EHL scales with the strength of the impurity coupling just as the Kondo screening length, ξ, does. Thus, in the gapless regime of the Kondo spin chain, our approach yields a method to detect the Kondo screening length [19, 21, 22] based on a true measure of entanglement. In addition, we *find* that entanglement in the Kondo regime is essentially unchanged if one rescales all the length scales with the EHL L^*.

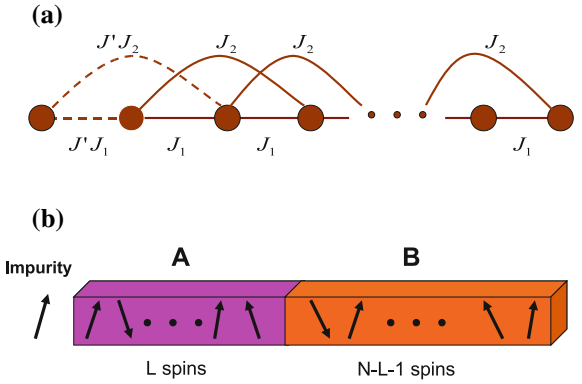

Fig. 3.3 (Color online) **a** Kondo Spin chain with next nearest neighbor Heisenberg interaction with one impurity at one end. **b** The chain is divided into three parts, an impurity, a block A and a block B. Entanglement is computed between the impurity and block B

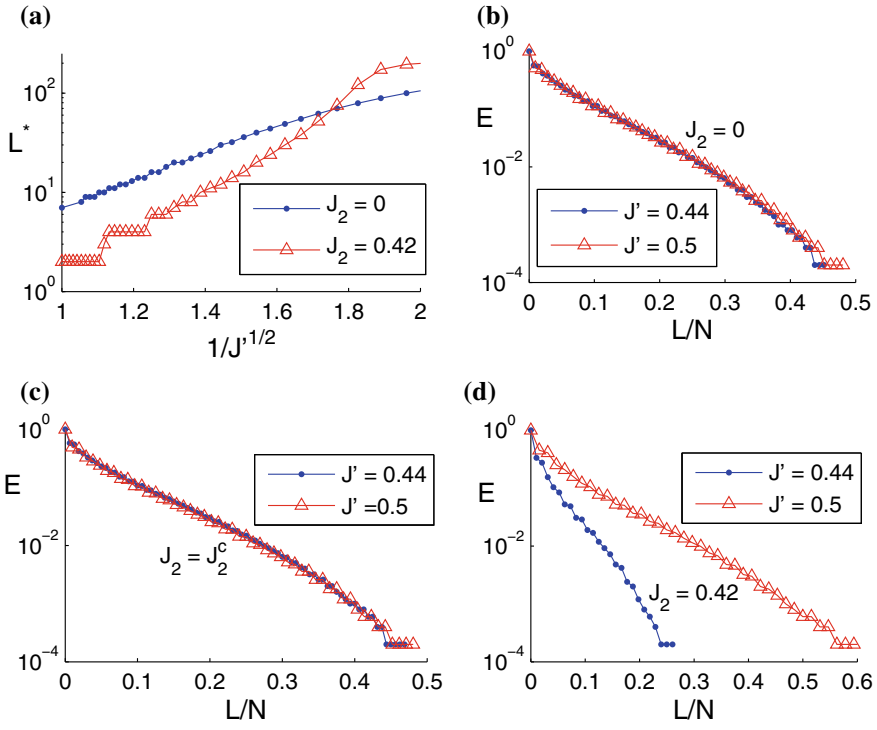

Fig. 3.4 (Color online) **a** L^* versus $1/\sqrt{J'}$ for both Kondo ($J_2 = 0$) and dimer regime ($J_2 = 0.42$). **b** Entanglement versus L/N for fixed $N/L^* = 4$ when $J_2 = 0$. **c** Entanglement versus L/N for fixed $N/L^* = 4$ at the critical point $J_2 = J_2^c$. **d** Entanglement versus L/N for fixed $N/L^* = 4$ in the dimer regime ($J_2 = 0.42$)

We find that there is an EHL L^* so that, for $L > L^*$, the entanglement between the impurity and block B is almost zero: L^* provides us with an estimate of the distance for which the impurity is mostly entangled with the spins contained in block A. For large chains ($N > 200$) in the Kondo regime, one finds that L^* is almost independent of N and depends only on J'. In the Kondo regime, i.e. for $J_2 < J_2^c$, L^* depends on J' just as the Kondo screening length ξ does [19, 20]; for small J', $L^* \propto e^{\alpha/\sqrt{J'}}$, where α is a constant. We plot L^* as a function of $1/\sqrt{J'}$ in Fig. 3.4a. In a semilogarithmic scale, the straight line plot exhibited in the Kondo regime ($J_2 = 0$) shows that L^* may be regarded as the Kondo screening length. Moreover, the nonlinearity of the same plot in the dimer regime ($J_2 = 0.42$), especially for small J', shows that, here, no exponential dependence on $1/\sqrt{J'}$ holds.

We observe also a remarkable scaling of negativity in the Kondo regime. This scaling may be regarded as yet another independent evidence of the fact that L^* is indeed the Kondo length ξ. In general, the entanglement E between the impurity and block B is a function of the three independent variables, J', L and N which, due to the one to one correspondence between J' and L^*, can be written as $E(L^*, L, N)$. We find that, in the Kondo regime, $E = E(N/L^*, L/N)$. To illustrate this, we fix the ratio N/L^* and plot the entanglement in terms of L/N for different values of J' (or equivalently L^*) for $J_2 = 0$ (Fig. 3.4b) and for $J_2 = J_2^c$ (Fig. 3.4c). The complete coincidence of the two plots in Figs. 3.4b and c shows that, in the Kondo regime, the spin chain can be scaled in size without essentially affecting the entanglement as long as L^* is also scaled. In the dimer regime the entanglement stays a function of three independent variables, i.e. $E = E(L^*, L, N)$, and, as shown in Fig. 3.4d, the entanglement does not scale with L^*. In our approach, the Entanglement Healing Length L^* may be evaluated in both the Kondo and the dimer regime: the scaling behavior, as well as the dependence of L^* on J', discriminates then between the very different entanglement properties exhibited by the spin chain Kondo model as J_2 crosses J_2^c.

We defined L^* such that there is no entanglement between the impurity and block B when block A is made of L^* spins. Conventional wisdom based on previous renormalization group analysis suggests that, in both regimes, the impurity and the block A of length L^* form a pure entangled state, while block B is also in a pure state. This is indeed approximately true in the dimer regime (exactly true for $J_2 = 0.5$) but it turns out to be dramatically different in the Kondo regime. To check this, [17] also computed the von Neumann entropy of the block B when block A has L^* spins and found it to be non zero. Thus, the blocks A and B are necessarily entangled in the Kondo regime as there is no entanglement between the impurity and B. In fact, after a distance L^*, the impurity is "screened" i.e, the block B feels as if it is part of a conventional gapless chain and has a diverging von Neumann entropy. The Kondo cloud is maximally entangled with the impurity as well as being significantly entangled with block B. Based on the above, a simple ansatz for the ground state $|GS\rangle$ in the Kondo regime is provided by

$$|GS\rangle = \sum_i \alpha_i \frac{|\uparrow\rangle|L_i^{\uparrow}(J')\rangle - |\downarrow\rangle|L_i^{\downarrow}(J')\rangle}{\sqrt{2}} \otimes |R_i(J')\rangle, \tag{3.12}$$

where α_i are constants, $\{|L_i^{\uparrow}(J')\rangle, |L_i^{\downarrow}(J')\rangle\}$ and $\{|R_i(J')\rangle\}$ are sets of orthogonal states on the cloud and the remaining system, respectively. At the fixed point $J' \to 0$ all spins except the impurity are included in $|L_i^{\uparrow}(J')\rangle$ and $|L_i^{\downarrow}(J')\rangle$. At $J' \to 1$, very few spins are contained in $|L_i^{\uparrow}(J')\rangle$ and $|L_i^{\downarrow}(J')\rangle$ while $\{|R_i(J')\rangle\}$ represents most of the chain.

The above exercise illustrates the efficacy of Negativity as a mixed state entanglement measure to capture emergent structures in many-body states such as the Kondo cloud, and use that to infer variational representations of the states.

3.4 Schmidt Gap for Signalling Quantum Criticality: Case Study with an Impurity Phase Transition

We now move to studying another quantity, the Schmidt gap, as defined in Sect. 3.1, which, although not a bonafide measure of entanglement, is an indicator of the same. It is extremely useful as an indicator of quantum phase transitions which do not have a local order parameter, such as generic impurity quantum phase transitions in which it is only the entanglement structure of the ground state which is re-arranged as one crosses the critical point.

As case study we again turn to a Kondo model, but now with *two* localized spin-1/2 impurities, coupled to the spins of the conduction electrons by an antiferromagnetic Kondo interaction and to each other via a Ruderman–Kittel–Kasuya–Yosida (RKKY) interaction. This is the *two-impurity Kondo model* [25], a theoretical workhorse in the study of impurity quantum phase transitions. When the Kondo interaction dominates, the electron spins screen the impurity spins (similar to the screening of a single spin-1/2 impurity in the ordinary Kondo model), while in the opposite limit the two impurity spins form a local singlet. The crossover between the two regimes sharpens into a quantum phase transition when each impurity is connected to its own distinct reservoir of conduction electrons [26]. The resulting "non-Fermi liquid" response of transport and thermodynamic observables has attracted much attention, with the first experiment reported in 2015 [27]. The lack of an easily identifiable local order parameter which exhibits scaling at the phase transition has triggered a search for alternative markers of the transition, the Schmidt gap being one viable candidate [28].

For a numerical computation of the Schmidt gap, using a Density Matrix Renormalization Group (DMRG) approach, it is convenient to first map the spin sector of the two-impurity Kondo model onto a spin chain, similar to what was done in the previous section for the ordinary Kondo model. One thus obtains a Hamiltonian $H = \sum_{m=L,R} H_m + H_I$, where

$$H_m = J'_m \left(J_1 \sigma_1^m \cdot \sigma_2^m + J_2 \sigma_1^m \cdot \sigma_3^m\right) + J_1 \sum_{i=2}^{N_m - 1} \sigma_i^m \cdot \sigma_{i+1}^m + J_2 \sum_{i=2}^{N_m - 2} \sigma_i^m \cdot \sigma_{i+2}^m, \qquad (3.13)$$

$$H_I = J_1 K \sigma_1^L \cdot \sigma_1^R.$$

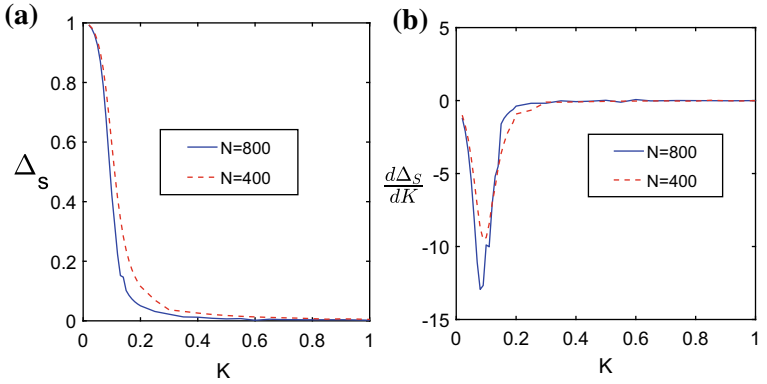

Fig. 3.5 **a** Schmidt gap as a function of the RKKY coupling K for different system sizes. **b** The derivative of the Schmidt gap with respect to the RKKY coupling K which shows non-analytic behavior as the system size increases. The figures are taken from [28]

Here $m = L, R$ labels two chains, denoted "left" and "right" respectively, with σ_i^m the vector of Pauli matrices at site i in chain m, and with J_1 (J_2) nearest- (next-nearest-) neighbor spin-exchange amplitudes. The parameters $J'_L > 0$ and $J'_R > 0$ play the role of antiferromagnetic Kondo couplings, with K the RKKY coupling between the impurity spins σ_1^L and σ_1^R. The total number of sites is thus $N = N_L + N_R$. Similar to the spin chain representation of the ordinary Kondo model, the ratio J_2/J_1 is fine tuned to the dimerization point $(J_2/J_1)_c = 0.2412$ of the spin chain [29], in this way killing off logarithmic corrections to the numerical finite-size data. In Fig. 3.5a we plot the Schmidt gap Δ_S (cf. Sect. 1) as a function of the RKKY coupling K when the system is cut across the bond between the two impurities. In other words, we regard the left (or right) chain as a subsystem of the full composite chain. As seen in the figure, the order-parameter-like profile of Δ_S becomes sharper as the size N of the chain increases, suggesting that Δ_S drops to zero at some critical value, $K = K_c$ in the thermodynamic limit. The interpretation of K_c as a critical point is evidenced by the sharp cusp of $\partial\Delta_S/\partial K$ at K_c as seen in Fig. 3.5b, with the cusp serving as a finite-size precursor of a critical non-analyticity in Δ'_S in the thermodynamic limit. Moreover, as shown in [28], by monitoring how the cusps move as functions of the Kondo coupling J', one finds, for sufficiently large systems, an almost perfect fit to the known exponential scaling of the quantum critical point $K_c \sim \exp(-\alpha/J')$ of the two-impurity Kondo model (with α a positive constant) [30]. It may be worth pointing out that cuts taken far away from the impurities yield Schmidt gaps which depend only weakly on the RKKY coupling, as expected from the local character of the transition [28]. Such cuts are thus less useful for spotting an impurity quantum phase transition.

A finite-size scaling analysis, with the Ansatz

$$\Delta_S = N^{-\beta/\nu} f_{\Delta_S}(|K - K_c|N^{1/\nu}), \tag{3.14}$$

gives further support for using the Schmidt gap Δ_S as a stand-in for a conventional order parameter. Here f_{Δ_S} is a scaling function, with β and δ the critical exponents governing the scaling of Δ_S and the crossover scale ξ [31] at the critical point: $\Delta_S \sim |K - K_c|^{\beta}$ and $\xi \sim |K - K_c|^{-\nu}$ respectively. The choice $\beta = 0.2 \pm 0.05$ and $\nu = 2 \pm 0.1$ yields a near-perfect data collapse when plotting $N^{\beta/\nu}\Delta_S$ as a function of $|K - K_c|N^{1/\nu}$ for different N and different impurity couplings J' [28]. The value $\nu = 2$ agrees with results from conformal field theory [32].

To summarize, DMRG data on the two-impurity Kondo model strongly suggests that the Schmidt gap faithfully captures its critical behavior. It is important to note that while the Schmidt gap is a nonlocal quantity, it can be represented as a superposition of n-point spin correlation functions, and therefore, in principle, be measured. To carry this out in an experiment clearly remains a challenge for the future. In the meantime, it would be interesting to attempt a characterization of impurity quantum phase transitions for other models using the Schmidt gap.

3.5 Entanglement Negativity as a Measurable Entity

In fact, the measure of negativity that we have used in large part of this article to quantify the entanglement, is also a measurable entity and one can accomplish it as long as one has the experimental access to several replicas of a system. In this section we show how to estimate logarithmic negativity using experimentally measurable quantities.

Logarithmic Negativity: For a generic mixed state, logarithmic negativity [5–8] is an entanglement measure. As logarithmic negativity does not rely on usual optimization over Hilbert space, needed in other entanglement measures, is computable efficiently. For a generic mixed state ρ_{AB} which explain the quantum state of two subsystems A and B the logarithmic negativity is defined as It is defined as:

$$\mathscr{E} = \log_2 \left|\rho_{AB}^{T_A}\right| = \log_2 \left|\rho_{AB}^{T_B}\right| = \log_2 \sum_k |\lambda_k| \tag{3.15}$$

with $|\cdot|$ the trace norm, $\rho_{AB}^{T_X}$ the partial transpose with respect to subsystem X, and $\{\lambda_k\}$ the eigenvalues of $\rho_{AB}^{T_X}$. Because of the non-trivial dependence of $\mathscr{E}$ on ρ_{AB}, there is no state-independent observable that can measure it—generally demanding full state tomography. The $\{\lambda_k\}$ are the roots of the characteristic polynomial, $P(\lambda) = \det(\lambda - \rho_{AB}^{T_B}) = \sum_n c_n \lambda^n$, where each c_n is a polynomial function of the partially transposed moments:

$$\mu_m = Tr[(\rho_{AB}^{T_B})^m] = \sum_k \lambda_k^m. \tag{3.16}$$

This means that, $\{\mu_m\}$ contains full information about the spectrum $\{\lambda_k\}$. Interestingly, even though partially transposed density matrices are generically unphysical,

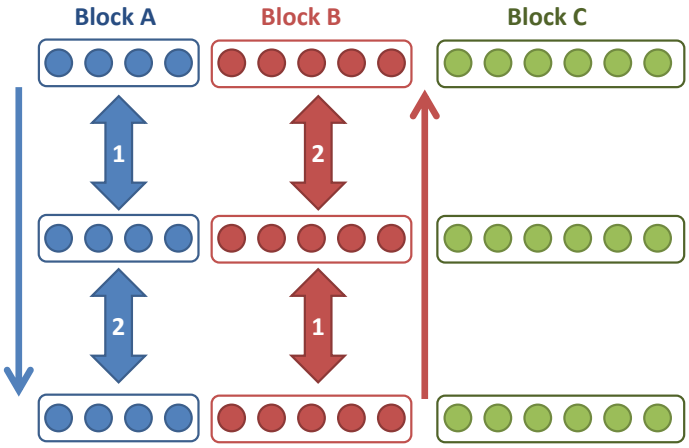

Fig. 3.6 Schematics: Example measurement set-up for the moments, $\mu_m = Tr[(\rho_{AB}^{T_B})^m]$, here for $m = 3$, from which one can extract the logarithmic negativity $\mathscr{E}$ between A and B. The generic mixedness of ρ_{AB} could arise from entanglement with environment C. Here the subsystems contain N_A, N_B and N_C particles respectively. The scheme involves three copies of the original system, and two counter propagating sets of measurements on A and B, ordered by the shown numbers, with direction depicted by the filled arrows

measurement of their moments is possible. In fact, there area few proposals in the literature for computing the the moments μ_m using m copies of the system. This includes, replica techniques [15] proposed for conformal field theory models, exploiting controlled swap operators between the copies [33, 34] and counter propagating swap measurements [35]. In the following, we provide a brief review of how to measure the moments based on the scheme of [35].

Measuring the Moments of $\rho_{AB}^{T_B}$: Here, we show that any moment can be measured using only SWAP-operators between the *individual* constituents of the m copies of the state ρ_{AB}, namely $\rho_{AB}^{\otimes m} = \bigotimes_{c=1}^{m} \rho_{A_cB_c}$. This general set-up is shown in Fig. 3.6, where the mixedness of ρ_{AB} arises from possible entanglement with a third system C, such that $\rho_{AB} = Tr_C|\Psi_{ABC}\rangle\langle\Psi_{ABC}|$ with $|\Psi_{ABC}\rangle$ being a pure tripartite state. The first step is to write the matrix power as an expectation of a permutation operator on the partially transposed copies:

$$\begin{aligned}\mu_m &= Tr[(\bigotimes_{c=1}^{m} \rho_{A_cB_c}^{T_{B_c}})P^m] \\ &= Tr[(\bigotimes_{c=1}^{m} \rho_{A_cB_c})(P^m)^{T_B}]\,,\end{aligned} \tag{3.17}$$

where P^m is any linear combination of cyclic permutation operators of order m and the second line makes use of the identity $Tr(\rho_{AB}^{T_B} O) = Tr(\rho_{AB} O^{T_B})$, valid for any operator O. A schematic of the equality in (3.17) for $m = 3$ is shown in Fig. 3.6. For

spin lattices, our choice of P^m to measure the moments μ_m results to the following steps in practice:

1. prepare m copies of the state ρ_{AB};
2. sequentially measure a 'forward' sequence of adjacent swaps, $S_A^{c,c+1}$ between neighbouring copies of system A from $c = 1$ to $m - 1$;
3. sequentially measure a 'backward' sequence of adjacent swaps, $S_B^{c,c-1}$ between neighbouring copies of system B from $c = m$ to 2;
4. repeat these steps in order to yield an expectation value.

This procedure is also depicted for $m = 3$ in Fig. 3.6. For each $m \leq 2$ we require $\mathcal{O}(N_A + N_B)$ measurements. This is in stark contrast to tomography, which generically for qubit systems requires $2^{2(N_A+N_B)}$ measurement settings. It is also worth emphasizing the difference between this procedure and other operational methods for measuring Renyi entropies [36–38]. First of all, Renyi entropies only quantify entanglement for pure states, and cannot be used in the more general mixed state scenario. Secondly, while for entropies the operations are only performed on a single subsystem, here, one performs both 'forward' and 'backward' operations on two subsystems at once, as explained above.

Estimating the logarithmic negativity from the moments of μ_m: To estimate the logarithmic negativity, a precise knowledge of all λ_k is not required. Since $-\frac{1}{2} \leq \lambda_k \leq 1$ for all k [39] and $\sum_k \lambda_k = 1$, generically, the magnitude of the moments quickly decreases with m, with the first few carrying the most information. This is crucial to help computing the logarithmic negativity with measuring only very few moments. One approach using only the even moments has been proposed in the quantum field theory literature [15] by exploiting numerical extrapolation. However, this method neglects the odd moments and generally requires a large number of moments and thus copies. In [35], it has been shown that the moments required, $\{\mu_m : m \leq M\}$, to accurately estimate the entanglement can number as few as $M = 3$. This is achieved by avoiding reconstruction of the spectrum or state and instead employing machine learning to directly map moments to logarithmic negativity. Note that μ_0 is simply the dimension of the systems Hilbert space, while $\mu_1 = 1$ in all cases. Additionally, it can be easily shown that μ_2 is equal to the purity of the state $= Tr[\rho_{AB}^2]$, and as such, $M \geq 3$ is needed to extract any information about $\mathscr{E}$. Therefore, using $M = 3$ copies is optimal in terms of resources.

Machine Learning Entanglement: Machine learning is as a key tool for modeling an unknown non-linear map between sets of data. In the supervised machine learning setup, one trains a model with a set of known inputs and their corresponding outputs. Once trained, the model can then be used to predict the unknown output of new input data. We follow the machine learning algorithm of the [35] for estimating the logarithmic negativity from the information contained in the moments, μ_m. The moments μ_m are taken as the input and the logarithmic negativity $\mathscr{E}$ as the output for training a deep neural networks [40, 41]. Training is performed by taking a large set of states for which μ_m and $\mathscr{E}$ can be computed on a classical computer. This model can then be used to predict $\mathscr{E}$ from a set of experimentally measured moments.

Training the neural network with random states: From an entanglement perspective, relevant states in condensed matter physics can be classified as either area-law, or volume-law. In the first case, the entanglement of a subsystem A with the rest is proportional to the number of qubits along their boundary. In the second, this entanglement is instead proportional to N_A, the number of qubits in A. Area-law states arise as low energy eigenstates of local gapped Hamiltonians, with logarithmic corrections in critical systems. Volume-law states however, are associated with the eigenstates found in the mid-spectrum, and as such arise in non-equilibrium dynamics. In order to train a neural network, a set of suitable training states, including both volume and area law quantum states, are required for which both the moments and logarithmic negativities are known. To encompass both area- and volume-law states, we consider two classes of states $|\Psi_{ABS}\rangle$: (i) random generic pure states (R-GPS), e.g. sampled from the Haar measure, which typically have volume-law entanglement [42, 43]; (ii) random matrix product states (R-MPS) with fixed bond dimension, which satisfy an area-law by construction [44]. In order to generate a training set with a wide range of entanglement features, subsystem sizes, and mixedness, we perform the following procedure:

1. For a fixed number of qubits N, take either a R-GPS, or R-MPS with bond dimension D.
2. Take different tri-partitions such that $N = N_A + N_B + N_C$, and for each calculate μ_m and $\mathscr{E}$ for ρ_{AB}.
3. Repeat for different random instances, while separately varying N and D.

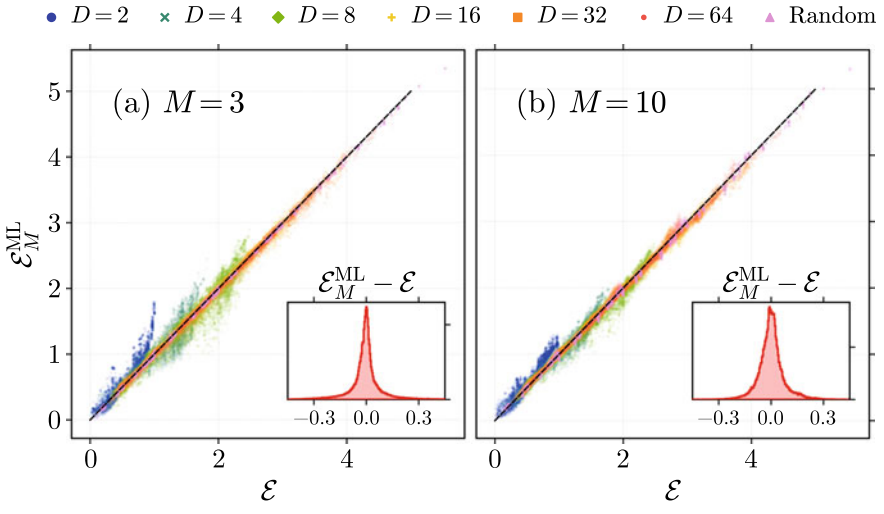

Fig. 3.7 Machine learning entanglement. Estimated logarithmic negativity $\mathscr{E}_M^{\mathrm{ML}}$, using a machine learning versus actual logarithmic negativity $\mathscr{E}$, for the same set of random states described in the main text. Training and prediction is performed using the moments μ_m generated from: **a** $M = 3$ copies; **b** $M = 10$ copies. The respective insets show the distribution of error, $\mathscr{E}_M^{\mathrm{ML}} - \mathscr{E}$. The figure is taken from the [35]

To check the performance of the neural network, we take the set of random states and split it in two, one half for training the neural network model, and the other as 'unseen' test data. In Fig. 3.7a we plot the machine learning model's predictions, $\mathscr{E}_M^{\mathrm{ML}}$, for the test data, using only $M = 3$ copies, in which a high degree of accuracy is achieved. In the inset of Fig. 3.7a, we plot a histogram of the errors $\mathscr{E}_M^{\mathrm{ML}} - \mathscr{E}$, which displays a very sharp peak at zero error with standard deviation ~ 0.09 A further improvement, particularly in outliers, is achieved by increasing the number of copies M to 10, see Fig. 3.7b, where the error standard deviation decreases to ~ 0.07. Regardless, the machine learning method is already very accurate for extracting entanglement using only three copies.

3.6 Conclusions

We have reviewed here the study of entanglement in many-body systems from an angle which is slightly different from the bulk of the literature. Most of the literature has concentrated on the entanglement between two complementary blocks in a many-body system or a quantum field theory. On the other hand, if we were to examine entanglement between two non-complementary parts of a system, this strategy will not work—in those cases concurrence and, for arbitrary dimensional systems, negativity, has to be employed. We have exemplified that study with examples: thermal entanglement and evidencing the Kondo cloud as an "entanglement cloud" around the impurity spin. We have also presented a strategy of how negativity can actually be measured in a many-body system using replicas in the laboratory, and how machine-learning can be used to make this more efficient. On a different vein, we have also exemplified how the Schmidt gap, which is not an entanglement measure, but a somewhat broad-brush indicator of entanglement, can be used to identify impurity quantum phase transitions.

Acknowledgements We acknowledge discussions carried out at the Workshop on Strongly Coupled Field Theories for Condensed Matter and Quantum Information Theory, IIP, Natal, Brazil. Much of the original work presented was funded by: EPSRC grant EP/K004077/1; Swedish Research Council grant no. 621-2011-3942 and STINT grant IG 2011-2028; the ERC grant PACOMANEDIA; Ministry of Science, Technology and Innovation of Brazil; CNPq Bolsa de Produtividade em Pesquisa.

References

1. R. Horodecki, P. Horodecki, M. Horodecki, K. Horodecki, Rev. Mod. Phys. **81**, 865 (2009)
2. S. Popescu, D. Rohrlich, Phys. Rev. A **56**, R3319(R) (1997)
3. P. Calabrese, J. Cardy, B. Doyon, J. Phys. A **42**, 500301 (2009)
4. W.K. Wootters, Phys. Rev. Lett. **80**, 2245 (1998)
5. K. Zyczkowski, P. Horodecki, A. Sanpera, M. Lewenstein, Phys. Rev. A **58**, 883 (1998)
6. J. Lee, M. Kim, Y. Park, S. Lee, J. Mod. Opt. **47**, 2151 (2000)

7. M.B. Plenio, Phys. Rev. Lett. **95**, 090503 (2005)
8. G. Vidal, R.F. Werner, Phys. Rev. A **65**, 032314 (2002)
9. M.C. Arnesen, S. Bose, V. Vedral, Phys. Rev. Lett. **87**, 017901 (2001)
10. S. Sachdev (Cambridge University Press, Cambridge, 2001)
11. A. Osterloh, L. Amico, G. Falci, R. Fazio, Nature **416**, 608 (2002)
12. T.J. Osborne, M.A. Nielsen, Phys. Rev. A **66**, 032110 (2002)
13. H. Wichterich, J. Molina-Vilaplana, S. Bose, Phys. Rev. A **80**, 010304(R) (2009)
14. S. Marcovitch, A. Retzker, M.B. Plenio, B. Reznik, Phys. Rev. A **80**, 012325 (2009)
15. P. Calabrese, J. Cardy, E. Tonni, Phys. Rev. Lett. **109**, 130502 (2012)
16. A. Bayat, Phys. Rev. Lett. **118**, 036102 (2017)
17. A. Bayat, P. Sodano, S. Bose, Phys. Rev. B **81**, 064429 (2010)
18. I. Affleck, Lecture Notes. Les Houches (2008), arXiv:0809.3474
19. E.S. Sorensen, M.S. Chang, N. Laflorencie, I. Affleck, J. Stat. Mech., P08003 (2007); E. S. Sorensen, M. S. Chang, N. Laflorencie, I. Affleck, J. Stat. Mech. L01001 (2007)
20. N. Laflorencie, E.S. Srensen, M.S. Chang, I. Affleck, Phys. Rev. Lett. **96**, 100603 (2006)
21. H. Frahm, A.A. Zvyagin, J. Cond. Matt. **9**, 9939 (1997)
22. R.G. Pereira, N. Laflorencie, I. Affleck, B.I. Halperin, Phys. Rev. B **77**, 125327 (2008)
23. N. Laflorencie, E.S. Sorensen, I. Affleck, J. Stat. Mech. **P0**, 2008 (2007)
24. M. Vojta, Phil. Mag. **86**, 1807 (2006)
25. C. Jayaprakash, H.-R. Krishnamurthy, J. Wilkins, Two-impurity Kondo problem. Phys. Rev. Lett. **47**, 737–740 (1981)
26. G. Zaránd, C.-H. Chung, P. Simon, M. Vojta, Phys. Rev. Lett. **97**, 166802 (2006)
27. A. Spinelli, M. Gerrits, R. Toskovic, B. Bryant, M. Ternes, A.F. Otte, Nat. Commun. **6**, 10046 (2015)
28. A. Bayat, H. Johannesson, S. Bose, P. Sodano, Nat. Commun. **5**, 3784 (2014)
29. K. Okamoto, K. Nomura, Phys. Lett. A **169**, 433 (1992)
30. B.A. Jones, C.M. Varma, Phys. Rev. B **40**, 324 (1989)
31. E. Sela, A.K. Mitchell, L. Fritz, Phys. Rev. Lett. **106**, 147202 (2011)
32. I. Affleck, A.W.W. Ludwig, B.A. Jones, Phys. Rev. B **52**, 9528 (1995)
33. H.A. Carteret, Phys. Rev. Lett. **94**, 040502 (2005)
34. K. Bartkiewicz, P. Horodecki, K. Lemr, A. Miranowicz, K. Zyczkowski, Phys. Rev. A **91**, 032315 (2015)
35. J. Gray, L. Banchi, A. Bayat, S. Bose, Phys. Rev. Lett. **121**, 150503 (2018)
36. A. Daley, H. Pichler, J. Schachenmayer, P. Zoller, Phys. Rev. Lett. **109**, 020505 (2012)
37. L. Banchi, A. Bayat, S. Bose, Phys. Rev. B **94**, 241117 (2016)
38. D.A. Abanin, E. Demler, Phys. Rev. Lett. **109**, 020504 (2012)
39. S. Rana, Phys. Rev. A **87**, 054301 (2013)
40. R. Rojas, *Neural Networks: A Systematic Introduction* (Springer Science and Business Media, Berlin, 2013)
41. J. Schmidhuber, Neural Netw. **61**, 85 (2015)
42. S. Popescu, A.J. Short, A. Winter, Nat. Phys. **2**, 754 (2006)
43. A. Hamma, S. Santra, P. Zanardi, Phys. Rev. Lett. **109**, 040502 (2012)
44. U. Schollwöck, Ann. Phys. **326**, 96 (2011)